International Journal of Fracture 39: 129–146 (1989)

The three-dimensional stress field around a cylindrical inclusion in a plate of arbitrary thickness

F.E. PENADO[1] and E.S. FOLIAS[2]
[1]*Division of Design and Analysis, Hercules Aerospace Co., Magna, Utah 84044, USA;* [2]*Department of Mechanical Engineering, University of Utah, Salt Lake City, Utah 84112, USA*

Received 1 November 1987; accepted in revised form 1 April 1988

Abstract. The three-dimensional Navier's equations are solved analytically for the case of a cylindrical inclusion of radius "a" which is embedded in a plate of arbitrary thickness $2h$. Both the plate and the inclusion are assumed to be of homogeneous and isotropic materials with different material properties. Perfect bonding is assumed to prevail at the interface. As to loading, a uniform tension is applied in the plane of the plate at points remote from the inclusion.

The analysis shows all stresses including the octahedral shear stress to be sensitive to the radius to half thickness ratio (a/h) as well as the material properties. In the limit, as $(\mu_2/\mu_1) \to 0$ and as $(\mu_2/\mu_1) \to 1$ (where μ_2 and μ_1 are, respectively, the shear moduli of the inclusion and of the plate) the results for a cylindrical hole and a continuous plate are recovered. Similarly as $(a/h) \to \infty$ (very thin plate) the plane stress solution is recovered. Moreover, for $(\mu_2/\mu_1) > 1.0$ the presence of a stress singularity near the point of intersection of the inclusion and the free surface of the plate is confirmed by the numerical results.

1. Introduction

The three-dimensional stress field around a cylindrical inclusion which is embedded in a plate is of considerable importance to the field of fracture mechanics. For example, solutions of this type can help us to understand better the failure mechanism in fiber-reinforced materials. Although an analytical solution to the title problem does not exist, related three-dimensional solutions can be found in the literature. These include an axially loaded rod partially embedded in an elastic half space for the cases of the elastic [1] or rigid [2] rod. The absence of a solution to the problem under consideration is not due to a lack of interest, but rather to the mathematical complexities encountered in solving this kind of three-dimensional problem. Thus, the purpose of this paper is twofold: first, to provide an analytical model for an isolated fiber in a matrix under uniaxial transverse tension; second to lay out the mathematical foundations that will allow the solution of similar three-dimensional problems in elasticity.

Two-dimensional solutions (plane stress or plane strain) for plates with perfectly bonded circular inclusions can be found in the literature for single [3] as well as multiple inclusions [4]. Reference [4] is an extension of the single inclusion case obtained by using the Schwarz method of successive approximations. Other related two-dimensional solutions involving a smooth (frictionless) circular inclusion that does not separate from its surrounding plate are found in [5] and [6] and correpond, respectively, to cases where the diameter of the inclusion is the same or larger than that of the hole in the plate. It was assumed in [5] and [6] that the plate and inclusion were of the same material. The case when a smooth circular inclusion separates from a plate of different material properties is discussed in [7].

Two-dimensional asymptotic solutions for the stresses in two bonded wedges of dissimilar materials in the neighborhood of the intersection of the free and bonded edges are found in [8] for orthogonal wedges, and in [9] for wedges of an arbitrary angle. The analysis shows that the stresses are proportional to $\varrho^{-\alpha}$, where α depends on the shear moduli ratio and the two Poisson's ratios. The largest value of α found in [8] was 0.311 and occurred for the case of one material being rigid and the other incompressible. Recently, Folias [10] used a three-dimensional analysis to investigate the asymptotic behavior of the stresses in the neighborhood of the intersection of a cylindrical inclusion and the free surface of a plate. The analysis shows the stresses to be singular for $\mu_2/\mu_1 > 1$ (where μ_2 and μ_1 are, respectively, the shear moduli of the inclusion and of the plate), with the strength of the singularity increasing as the ratio μ_2/μ_1 increases.

2. Formulation of the problem

Consider the equilibrium of a body which occupies the space $|x| < \infty, |y| < \infty, |z| \leqslant h$ and contains two regions of different elastic properties. Their common boundary consists of a through-the-thickness cylindrical surface of radius $r = a$, whose generators are parallel to the z-axis (see Fig. 1). The regions $r \geqslant a$ and $r \leqslant a$ are called, respectively, plate and inclusion and are denoted by the superscripts (1) and (2). Both the plate and the inclusion are considered to be made of homogeneous, isotropic and linearly elastic materials. At the

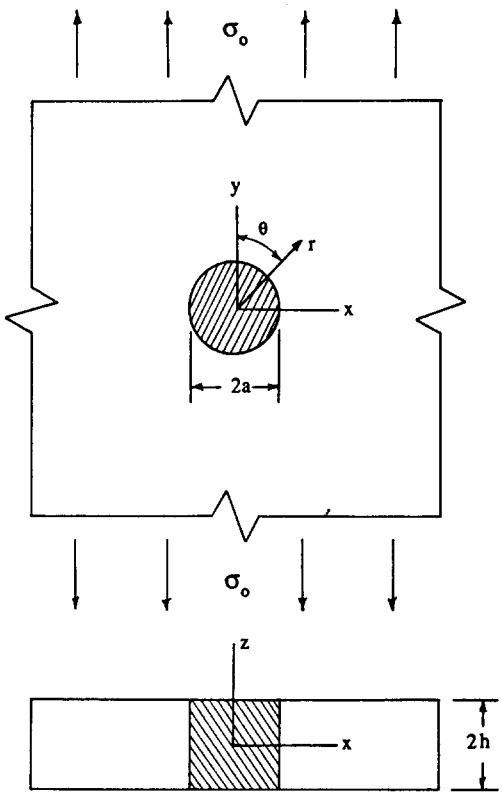

Fig. 1. Infinite plate of arbitrary thickness with cylindrical inclusion.

interface ($r = a$) perfect bonding is assumed to prevail. As to loading, a uniform tension σ_0 is applied at the boundary of the plate at points remote from the inclusion. For both regions, the surfaces $|z| = h$ are assumed to be free of stresses and constraints.

In the absence of body forces, the coupled differential equations governing the displacement functions $u^{(i)}$, $v^{(i)}$ and $w^{(i)}$ ($i = 1, 2$) are

$$\frac{m_i}{m_i - 2}\frac{\partial e^{(i)}}{\partial x_k} + \nabla^2 u_k^{(i)} = 0; \quad i = 1, 2; k = 1, 2, 3, \tag{1}$$

where ∇^2 is the $3D$ Laplacian operator, $m_i \equiv 1/\nu_i$, ν_i is Poisson's ratio and

$$e^{(i)} \equiv \frac{\partial u_k^{(i)}}{\partial x_k}; \quad k = 1, 2, 3. \tag{2}$$

The stress-displacement relations are given by Hooke's law as:

$$\sigma_{kl}^{(i)} = 2\mu_i \left\{\frac{1}{m_i - 2} e_{jj}^{(i)} \delta_{lk} + e_{lk}^{(i)}\right\}; \quad k, l = 1, 2, 3, \tag{3}$$

where μ_i are the respective shear moduli.

As to the boundary conditions, one must require that

$$\text{as } |x| \to \infty: \sigma_{xx}^{(1)} = \tau_{xy}^{(1)} = \tau_{xz}^{(1)} = 0 \tag{4}$$

$$\text{as } |y| \to \infty: \tau_{xy}^{(1)} = \tau_{yz}^{(1)} = 0, \sigma_{yy}^{(1)} = \sigma_0 \tag{5}$$

$$\text{at } |z| = h: \tau_{xz}^{(i)} = \tau_{yz}^{(i)} = \sigma_{zz}^{(i)} = 0; \quad i = 1, 2 \tag{6}$$

$$\text{at } r = a: \sigma_{rr}^{(1)} - \sigma_{rr}^{(2)} = \tau_{r\theta}^{(1)} - \tau_{r\theta}^{(2)} = \tau_{rz}^{(1)} - \tau_{rz}^{(2)} = 0 \tag{7}$$

$$u_r^{(1)} - u_r^{(2)} = u_\theta^{(1)} - u_\theta^{(2)} = u_z^{(1)} - u_z^{(2)} = 0. \tag{8}$$

Finally, at $r = 0$ we must require that all stresses and displacements be bounded.

It is found convenient at this stage to seek the solution to (1) in the form:

$$u^{(i)} = u^{(p)(i)} + u^{(c)(i)} \tag{9}$$

$$v^{(i)} = v^{(p)(i)} + v^{(c)(i)}; \quad i = 1, 2, \tag{10}$$

$$w^{(i)} = w^{(p)(i)} + w^{(c)(i)} \tag{11}$$

where the component with the superscript (p) represents the particular solution, and the component with the superscript (c) the complementary solution.

The particular solution in cylindrical coordinates is:

(i) for the plate:

$$u_{rr}^{(p)(1)} = \frac{\sigma_0 r}{4\mu_1}\left[\frac{1 - \nu_1}{1 + \nu_1} + \cos(2\theta)\right] \tag{12}$$

$$u_{\theta}^{(p)(1)} = -\frac{\sigma_0 r}{4\mu_1}\sin(2\theta) \tag{13}$$

$$u_{zz}^{(p)(1)} = -\frac{\sigma_0}{2\mu_1}\frac{\nu_1}{1+\nu_1}z \tag{14}$$

$$\sigma_{rr}^{(p)(1)} = \tfrac{1}{2}\sigma_0[1+\cos(2\theta)] \tag{15}$$

$$\sigma_{\theta\theta}^{(p)(1)} = \tfrac{1}{2}\sigma_0[1-\cos(2\theta)] \tag{16}$$

$$\tau_{r\theta}^{(p)(1)} = -\tfrac{1}{2}\sigma_0\sin(2\theta) \tag{17}$$

$$\tau_{rz}^{(p)(1)} = \tau_{\theta z}^{(p)(1)} = \sigma_{zz}^{(p)(1)} = 0 \tag{18}$$

(ii) for the inclusion:

$$u_{rr}^{(p)(2)} = C_1 r + C_2 r\cos(2\theta) \tag{19}$$

$$u_{\theta\theta}^{(p)(2)} = -C_2 r\sin(2\theta) \tag{20}$$

$$u_{zz}^{(p)(2)} = -2\frac{\nu_2}{1-\nu_2}C_1 z \tag{21}$$

$$\sigma_{rr}^{(p)(2)} = 2\mu_2\left[\frac{1+\nu_2}{1-\nu_2}C_1 + C_2\cos(2\theta)\right] \tag{22}$$

$$\sigma_{\theta\theta}^{(p)(2)} = 2\mu_2\left[\frac{1+\nu_2}{1-\nu_2}C_1 - C_2\cos(2\theta)\right] \tag{23}$$

$$\tau_{r\theta}^{(p)(2)} = -2\mu_2 C_2\sin(2\theta) \tag{24}$$

$$\tau_{rz}^{(p)(2)} = \tau_{\theta z}^{(p)(2)} = \sigma_{zz}^{(p)(2)} = 0, \tag{25}$$

where C_1 and C_2 are constants to be determined later from the boundary conditions at $r = a$. Note that the above particular solution for the inclusion satisfies the continuity conditions at $r = 0$.

In view of the particular solution, one needs to find six complementary displacements, i.e., $u^{(c)(i)}, v^{(c)(i)}, w^{(c)(i)}$ $(i = 1, 2)$, such that they satisfy the partial differential equation (1) and the following boundary conditions:

$$\text{at } |z| = h\text{: } \tau_{xz}^{(c)(i)} = \tau_{yz}^{(c)(i)} = \sigma_{zz}^{(c)(i)} = 0 \tag{26}$$

$$\text{at } r = a\text{: } \sigma_{rr}^{(c)(1)} - \sigma_{rr}^{(c)(2)} = -\sigma_{rr}^{(p)(1)} + \sigma_{rr}^{(p)(2)} \tag{27}$$

$$\tau_{r\theta}^{(c)(1)} - \tau_{r\theta}^{(c)(2)} = -\tau_{r\theta}^{(p)(1)} + \tau_{r\theta}^{(p)(2)} \tag{28}$$

$$\tau_{rz}^{(c)(1)} - \tau_{rz}^{(c)(2)} = -\tau_{rz}^{(p)(1)} + \tau_{rz}^{(p)(2)} = 0 \tag{29}$$

$$u_{rr}^{(c)(1)} - u_{rr}^{(c)(2)} = -u_{rr}^{(p)(1)} + u_{rr}^{(p)(2)} \tag{30}$$

$$u_{00}^{(c)(1)} - u_{00}^{(c)(2)} = -u_{00}^{(p)(1)} + u_{00}^{(p)(2)} \tag{31}$$

$$u_{zz}^{(c)(1)} - u_{zz}^{(c)(2)} = -u_{zz}^{(p)(1)} + u_{zz}^{(p)(2)}. \tag{32}$$

Moreover, in order to complete the formulation of the complementary problem we must require that:

$$\text{as } r \to \infty\text{: all complementary displacements and stresses for the plate must vanish} \tag{33}$$

and the continuity condition:

$$\text{at } r = 0\text{: all complementary displacements and stresses for the inclusion must be bounded.} \tag{34}$$

3. Method of solution

A general method for constructing solutions for some three-dimensional mixed boundary-value problems which arise in elastostatics was developed by Folias [11] who illustrated the method by applying it to the problem of a uniform extension of an infinite plate containing a through the thickness line crack. Later, Folias and Wang [12] specialized the general solution to the case of a plate of an arbitrary thickness containing a cylindrical hole. Based on these results, one can deduce that the general form of the solution to system (1) which automatically satisfies the boundary conditions at the plate faces, i.e. (26) is†:

$$\begin{aligned} u^{(c)(i)} = {} & \frac{1}{m_i - 2} \sum_{\nu=1}^{\infty} \frac{\partial^2 H_\nu^{(i)}}{\partial x^2} \{2(m_i - 1) f_1(\beta_\nu z) + m_i f_2(\beta_\nu z)\} \\ & + \sum_{n=1}^{\infty} \left\{ - \frac{\partial^2 H_n^{(i)}}{\partial x^2} + \alpha_n^2 H_n^{(i)} \right\} \cos(\alpha_n h) \cos(\alpha_n z) \\ & + \lambda_1^{(i)} - y \frac{\partial \lambda_3^{(i)}}{\partial x} + \frac{1}{m_i + 1} z^2 \frac{\partial^2 \lambda_3^{(i)}}{\partial x \partial y} \end{aligned} \tag{35}$$

† Note that because of symmetry in the present problem, one needs only to consider the region $0 \leqslant \theta \leqslant \pi/2$.

$$v^{(c)(i)} = \frac{1}{m_i - 2}\sum_{\nu=1}^{\infty}\frac{\partial^2 H_\nu^{(i)}}{\partial x\partial y}\{2(m_i - 1)f_1(\beta_\nu z) + m_i f_2(\beta_\nu z)\}$$
$$- \sum_{n=1}^{\infty}\frac{\partial^2 H_n^{(i)}}{\partial x\partial y}\cos(\alpha_n h)\cos(\alpha_n z) \tag{36}$$
$$+ \frac{3m_i - 1}{m_i + 1}\lambda_3^{(i)} + \lambda_2^{(i)} - y\frac{\partial\lambda_3^{(i)}}{\partial y} - \frac{1}{m_i + 1}z^2\frac{\partial^2\lambda_3^{(i)}}{\partial x^2}$$

$$w^{(c)(i)} = \frac{1}{m_i - 2}\sum_{\nu=1}^{\infty}\frac{\partial H_\nu^{(i)}}{\partial x}\beta_\nu\{(m_i - 2)f_3(\beta_\nu z) - m_i f_4(\beta_\nu z)\} - \frac{2}{m_i + 1}z\frac{\partial\lambda_3^{(i)}}{\partial y}. \tag{37}$$

Furthermore, the stresses are given by:

$$\frac{1}{2\mu_i}\sigma_{xx}^{(c)(i)} = \frac{1}{m_i - 2}\sum_{\nu=1}^{\infty}\left\{2\beta_\nu^2\frac{\partial H_\nu^{(i)}}{\partial x}f_1(\beta_\nu z)\right.$$
$$\left. + \frac{\partial^3 H_\nu^{(i)}}{\partial x^3}[2(m_i - 1)f_1(\beta_\nu z) + m_i f_2(\beta_\nu z)]\right\}$$
$$+ \sum_{n=1}^{\infty}\left\{-\frac{\partial^3 H_n^{(i)}}{\partial x^3} + \alpha_n^2\frac{\partial H_n^{(i)}}{\partial x}\right\}\cos(\alpha_n h)\cos(\alpha_n z) \tag{38}$$
$$+ \frac{\partial\lambda_1^{(i)}}{\partial x} - y\frac{\partial^2\lambda_3^{(i)}}{\partial x^2} + \frac{2}{m_i + 1}\frac{\partial\lambda_3^{(i)}}{\partial y} + \frac{1}{m_i + 1}z^2\frac{\partial^3\lambda_3^{(i)}}{\partial x^2\partial y}$$

$$\frac{1}{2\mu_i}\sigma_{yy}^{(c)(i)} = \frac{1}{m_i - 2}\sum_{\nu=1}^{\infty}\left\{2\beta_\nu^2\frac{\partial H_\nu^{(i)}}{\partial x}f_i(B_\nu z)\right.$$
$$\left. - \left(\frac{\partial^3 H_\nu^{(i)}}{\partial x^3} - \beta_\nu^2\frac{\partial H_\nu^{(i)}}{\partial x}\right)[2(m_i - 1)f_1(\beta_\nu z) + m_i f_2(\beta_\nu z)]\right\}$$
$$+ \sum_{n=1}^{\infty}\left\{\frac{\partial^3 H_n^{(i)}}{\partial x^3} - \alpha_n^2\frac{\partial H_n^{(i)}}{\partial x}\right\}\cos(\alpha_n h)\cos(\alpha_n z) \tag{39}$$
$$+ \frac{2m_i}{m_i + 1}\frac{\partial\lambda_3^{(i)}}{\partial y} - \frac{\partial\lambda_1^{(i)}}{\partial x} + y\frac{\partial^2\lambda_3^{(i)}}{\partial x^2} - \frac{1}{m_i + 1}z^2\frac{\partial^3\lambda_3^{(i)}}{\partial x^2\partial y}$$

$$\frac{1}{2\mu_i}\sigma_{zz}^{(c)(i)} = -\frac{m_i}{m_i - 2}\sum_{\nu=1}^{\infty}\frac{\partial H_\nu^{(i)}}{\partial x}\beta_\nu^2 f_2(\beta_\nu z) \tag{40}$$

$$\frac{1}{2\mu_i}\tau_{xy}^{(c)(i)} = \frac{1}{m_i - 2}\sum_{\nu=1}^{\infty}\frac{\partial^3 H_\nu^{(i)}}{\partial x^2\partial y}\{2(m_i - 1)f_1(\beta_\nu z) + m_i f_2(\beta_\nu z)\}$$
$$- \sum_{n=1}^{\infty}\left\{\frac{\partial^3 H_n^{(i)}}{\partial x^2\partial y} - \frac{1}{2}\alpha_n^2\frac{\partial H_n^{(i)}}{\partial y}\right\}\cos(\alpha_n h)\cos(\alpha_n z) \tag{41}$$
$$+ \frac{m_i - 1}{m_i + 1}\frac{\partial\lambda_3^{(i)}}{\partial x} + \frac{\partial\lambda_2^{(i)}}{\partial x} - y\frac{\partial^2\lambda_3^{(i)}}{\partial x\partial y} - \frac{1}{m_i + 1}z^2\frac{\partial^3\lambda_3^{(i)}}{\partial x^3}$$

$$\frac{1}{2\mu_i}\tau_{yz}^{(c)(i)} = -\frac{m_i}{m_i-2}\sum_{v=1}^{\infty}\frac{\partial^2 H_v^{(i)}}{\partial x\partial y}\beta_v\{f_3(\beta_v z)+f_4(\beta_v z)\} + \frac{1}{2}\sum_{n=1}^{\infty}\alpha_n\frac{\partial^2 H_n^{(i)}}{\partial x\partial y}\cos(\alpha_n h)\sin(\alpha_n z) \tag{42}$$

$$\frac{1}{2\mu_i}\tau_{xz}^{(c)(i)} = -\frac{m_i}{m_i-1}\sum_{v=1}^{\infty}\frac{\partial^2 H_v^{(i)}}{\partial x^2}\beta_v\{f_3(\beta_v z)+f_4(\beta_v z)\} + \frac{1}{2}\sum_{n=1}^{\infty}\left[\frac{\partial^2 H_n^{(i)}}{\partial x^2}-\alpha_n^2 H_n^{(i)}\right]\alpha_n\cos(\alpha_n h)\sin(\alpha_n z), \tag{43}$$

where

$$\alpha_n = \frac{n\pi}{h},\quad n = 1, 2, 3, \ldots, \tag{44}$$

β_v are the roots of the equation

$$\sin(2\beta_v h) = -(2\beta_v h), \tag{45}$$

$H_v^{(i)}$ and $H_n^{(i)}$ are functions of x and y which satisfy the reduced wave equation:

$$\left(\frac{\partial^2}{\partial x^2}+\frac{\partial^2}{\partial y^2}-\beta_v^2\right)\frac{\partial H_v^{(i)}}{\partial x} = 0 \tag{46}$$

$$\left(\frac{\partial^2}{\partial x^2}+\frac{\partial^2}{\partial y^2}-\alpha_n^2\right)\frac{\partial H_n^{(i)}}{\partial y} = 0, \tag{47}$$

$\lambda_1^{(i)}$, $\lambda_2^{(i)}$ and $\lambda_3^{(i)}$ are two dimensional harmonic functions, and

$$f_1(\beta_v z) \equiv \cos(\beta_v h)\cos(\beta_v z) \tag{48}$$

$$f_2(\beta_v z) \equiv \beta_v h\sin(\beta_v h)\cos(\beta_v z) - \beta_v z\cos(\beta_v h)\sin(\beta_v z) \tag{49}$$

$$f_3(\beta_v z) \equiv \cos(\beta_v h)\sin(\beta_v z) \tag{50}$$

$$f_4(\beta_v z) \equiv \beta_v h\sin(\beta_v h)\sin(\beta_v z) + \beta_v z\cos(\beta_v h)\cos(\beta_v z). \tag{51}$$

By virtue of its construction, the complementary solution automatically satisfies the boundary conditions at the plate faces $|z| = h$. It remains next to satisfy the boundary conditions on the surface of the inclusion.

Utilizing the appropriate coordinate transformations from rectangular to cylindrical coordinates, (27)–(32) can be written in the form:

$$\sin^2\theta(\sigma_{xx}^{(c)(1)}-\sigma_{xx}^{(c)(2)})+\cos^2\theta(\sigma_{yy}^{(c)(1)}-\sigma_{yy}^{(c)(2)})+\sin(2\theta)(\tau_{xy}^{(c)(1)}-\tau_{xy}^{(c)(2)}) = -\left[\frac{1}{2}\sigma_0 - 2\mu_2\frac{1+\nu_2}{1-\nu_2}C_1\right]-[\tfrac{1}{2}\sigma_0-2\mu_2 C_2]\cos(2\theta) \tag{52}$$

$$\tfrac{1}{2}\sin(2\theta)(\sigma_{xx}^{(c)(1)} - \sigma_{xx}^{(c)(2)}) - \tfrac{1}{2}\sin(2\theta)(\sigma_{yy}^{(c)(1)} - \sigma_{yy}^{(c)(2)}) + \cos(2\theta)(\tau_{xy}^{(c)(1)} - \tau_{xy}^{(c)(2)})$$

$$= [\tfrac{1}{2}\sigma_0 - 2\mu_2 C_2]\sin(2\theta) \tag{53}$$

$$\sin\theta(\tau_{xy}^{(c)(1)} - \tau_{xy}^{(c)(2)}) + \cos\theta(\tau_{yz}^{(c)(1)} - \tau_{yz}^{(c)(2)}) = 0 \tag{54}$$

$$\sin\theta(u^{(c)(1)} - u^{(c)(2)}) + \cos\theta(v^{(c)(1)} - v^{(c)(2)})$$

$$= -\left[\frac{\sigma_0 a}{4\mu_1}\frac{1-\nu_1}{1+\nu_1} - C_1 a\right] - \left[\frac{\sigma_0 a}{4\mu_1} - C_2 a\right]\cos(2\theta) \tag{55}$$

$$\cos\theta(u^{(c)(1)} - u^{(c)(2)}) - \sin\theta(v^{(c)(1)} - v^{(c)(2)}) = \left[\frac{\sigma_0 a}{4\mu_1} - C_2 a\right]\sin(2\theta) \tag{56}$$

$$w^{(c)(1)} - w^{(c)(2)} = \left[\frac{\sigma_0}{2\mu_1}\frac{\nu_1}{1+\nu_1} - \frac{2\nu_2}{1-\nu_2}C_1\right]z. \tag{57}$$

Examining the nature of (52)–(57), one notices that the θ-dependency can be eliminated by considering the following forms of the solution to (46)–(47):

$$\frac{\partial H_v^{(1)}}{\partial x} = c_{1v}K_0(\beta_v r) + c_{2v}K_2(\beta_v r)\cos(2\theta) \tag{58}$$

$$\frac{\partial H_v^{(2)}}{\partial x} = c_{3v}I_0(\beta_v r) + c_{4v}I_2(\beta_v r)\cos(2\theta) \tag{59}$$

$$\frac{\partial H_n^{(1)}}{\partial y} = c_{1n}K_0(\alpha_n r) + c_{2n}K_2(\alpha_n r)\sin(2\theta) \tag{60}$$

$$\frac{\partial H_n^{(2)}}{\partial y} = c_{3n}I_0(\alpha_n r) + c_{4n}I_2(\alpha_n r)\sin(2\theta) \tag{61}$$

$$\lambda_1^{(1)} = \frac{A}{r}\sin\theta - \frac{2Ba^2}{r^3}\sin(3\theta) \tag{62}$$

$$\lambda_2^{(1)} = \frac{A}{r}\cos\theta - \frac{2Ba^2}{r^3}\cos(3\theta) \tag{63}$$

$$\lambda_3^{(1)} = \frac{D}{r}\cos\theta \tag{64}$$

$$\lambda_1^{(2)} = E\,r\sin\theta \tag{65}$$

$$\lambda_2^{(2)} = -E\,r\cos\theta \tag{66}$$

$$\lambda_3^{(2)} = G\,r\cos\theta, \tag{67}$$

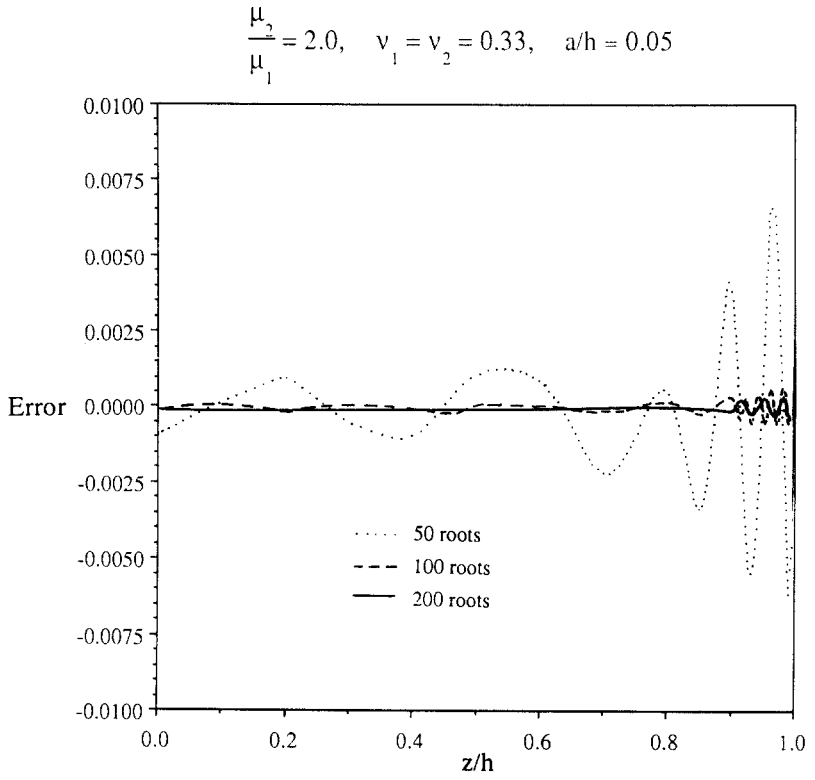

Fig. 2. Boundary condition across the thickness at $r = a$ for the stress $\tau_{r\theta}$ for $\mu_2/\mu_1 = 2.0$, $\nu_1 = \nu_2 = 0.33$ and $a/h = 0.05$.

where I_m and K_m ($m = 0, 2$) are, respectively, the modified Bessel functions of the first and second kind of order m, and c_{kv}, c_{kn} ($k = 1, 2, 3, 4$; $v, n = 1, 2, 3, \ldots$), A, B, D, E, G are arbitrary constants.

Finally, substituting (58)–(67) into (52)–(57) and letting $r = a$ one arrives at a system of six equations involving series in z. The system may then be solved numerically, by the method of [13], for the unknown coefficients. Details of the numerical solution can be found in [14]. Although the system is extremely sensitive to small changes in the coefficients, the method does furnish a solution which converges as the number of characteristic roots increases. The rate of convergence may be seen in Fig. 2 where the results for the boundary condition $\tau_{r\theta}$ for 50, 100 and 200 roots are plotted. This boundary condition was chosen because it is the most difficult one to satisfy. The reader should also notice that the little oscillation at the end is the result of the stress singularity which is present, for $\mu_2/\mu_1 = 2$, in the neighborhood of the point $z = h$ (see [10]).

As a check, the following three limiting cases will be examined:

(i) *Continuous plate.* If $\nu_1 = \nu_2$ and $\mu_2/\mu_1 = 1$, then the solutions for the plate and the inclusion reduce to the particular solution for the plate, i.e. (12)–(18).

(ii) *Thin plate.* If $h/a \to 0$, then one recovers precisely the plane stress solution given by Goodier [3].

(iii) *Cylindrical hole.* In this case $\mu_2/\mu_1 \to 0$. The stress $\sigma_{00}^{(1)}/\sigma_0$ was evaluated numerically for $\theta = \pi/2$, $\mu_2/\mu_1 = 0.000\,01$, $\nu_1 = \nu_2 = 0.33$ and different values of a/h. The results are

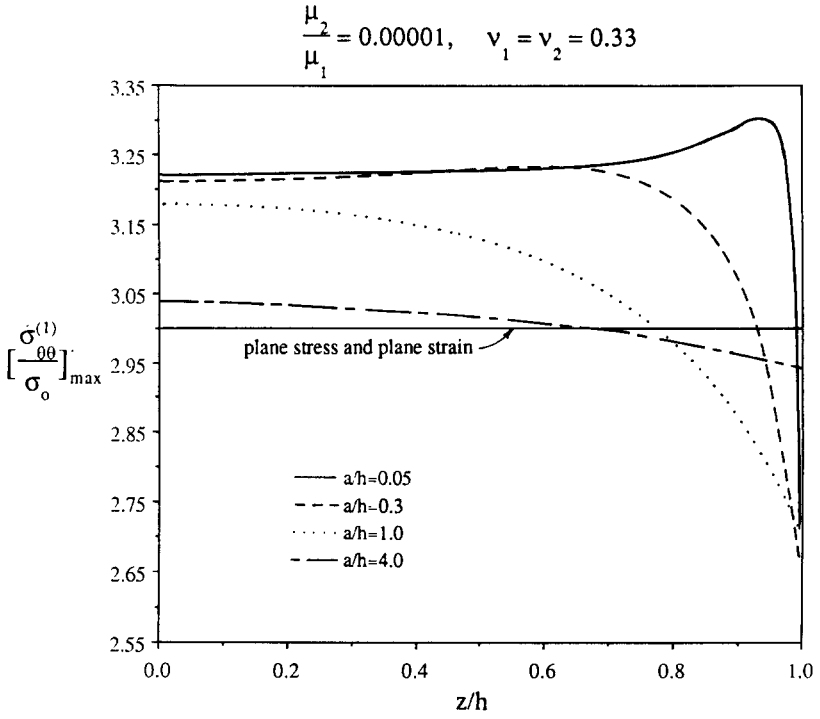

Fig. 3. Maximum normal stress for the plate across the thickness for $\mu_2/\mu_1 = 0.000\,01$ (cylindrical hole), $\nu_1 = \nu_2 = 0.33$ and different values of a/h.

shown in Fig. 3 where they are compared with those obtained by Folias and Wang [12]. The agreement is excellent indicating, therefore, that in the limit as $\mu_2/\mu_1 \to 0$ the present results tend to those obtained for a cylindrical hole.

4. Numerical results

Once the coefficients have been determined, the stresses and displacements may then be calculated at any point in the body. More specifically, we will calculate the stresses $\sigma_{\theta\theta}$, σ_{zz}, τ_{oct} and the out of the plane displacement u_{zz} and we will compare them with the results for plane stress and plane strain obtained in [3].

To quantify the effect that the applied load has upon failure, we choose as a suitable parameter the octahedral shear stress for it is directly related to the von Mises criterion, i.e.

$$\tau_{oct} = \frac{\sqrt{2}}{3}\sigma_Y, \tag{68}$$

where σ_Y represents the yield stress in simple tension.

Equation (68) describes the locus of the points in the composite plate where τ_{oct} attains a high value which may lead to failure initiation. Figures 4–7 show the maximum octahedral shear stress for the plate as a function of z/h, for different values of the thickness parameter, a/h, and the shear moduli ratio, μ_2/μ_1. The maximum value of τ_{oct} occurs at $r = a$ and $\theta = 0$

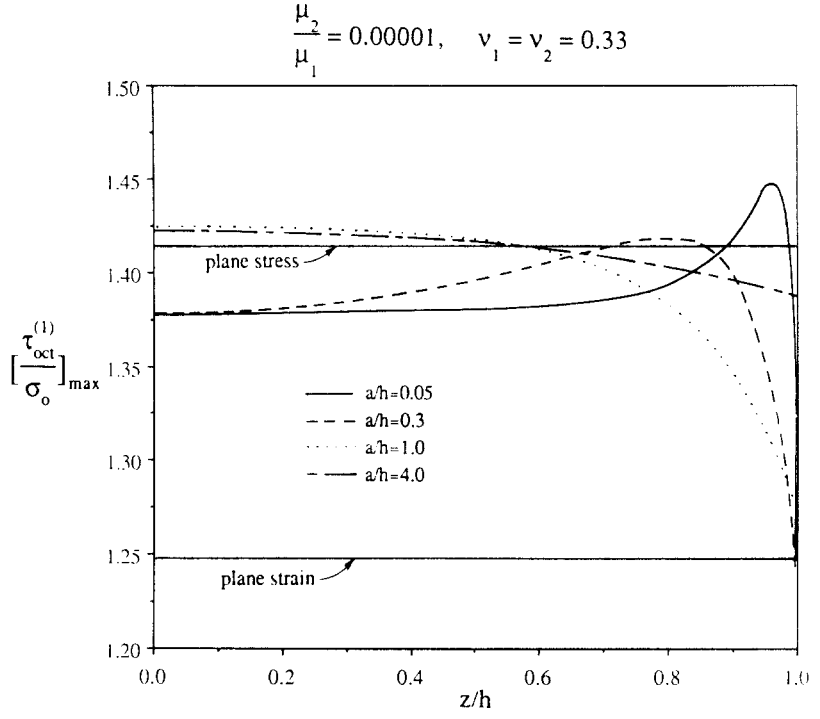

Fig. 4. Maximum octahedral shear stress for the plate across the thickness for $\mu_2/\mu_1 = 0.000\,01$ (cylindrical hole), $\nu_1 = \nu_2 = 0.33$ and different values of a/h.

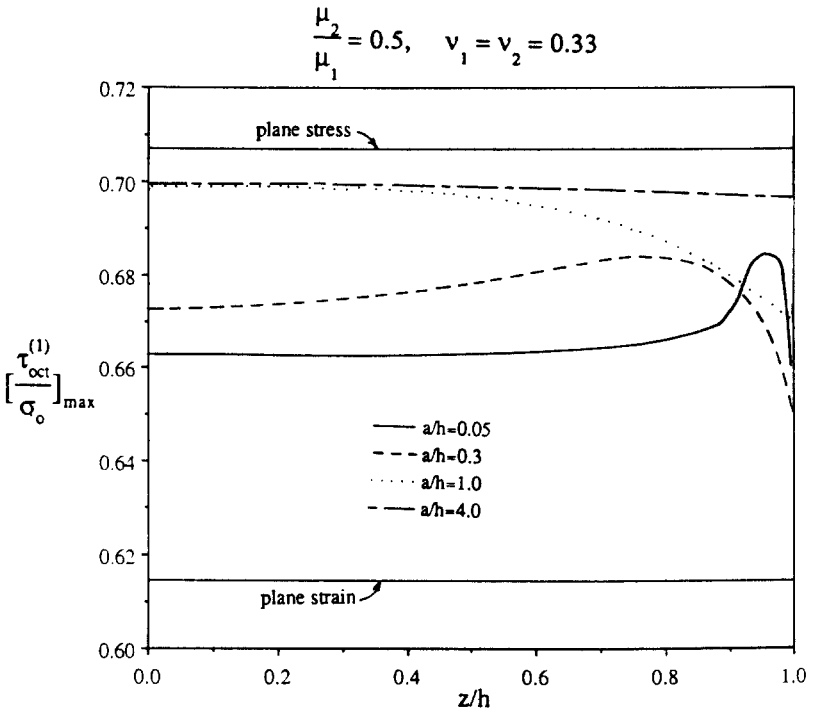

Fig. 5. Maximum octahedral shear stress for the plate across the thickness for $\mu_2/\mu_1 = 0.5$, $\nu_1 = \nu_2 = 0.33$ and different values of a/h.

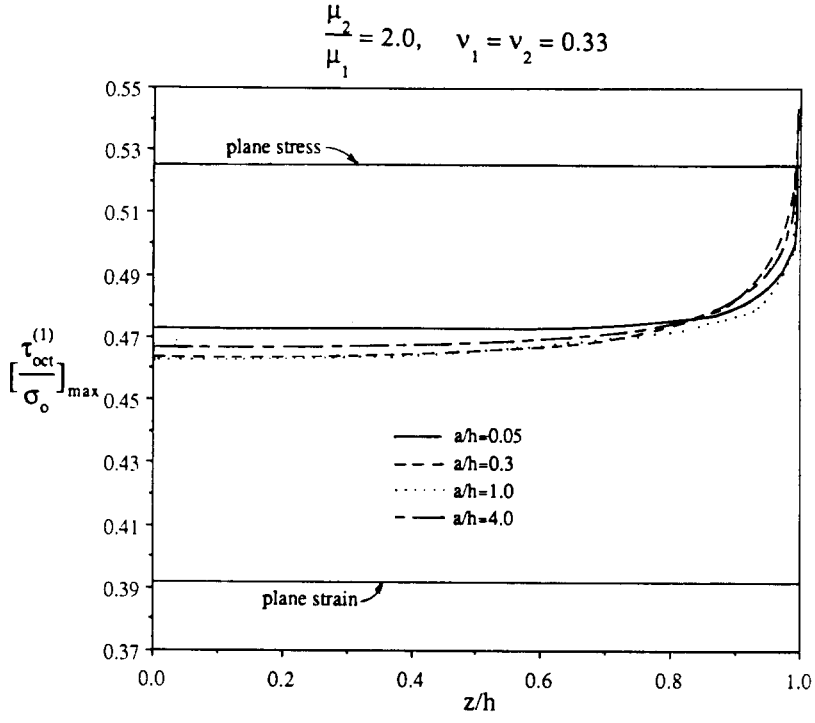

Fig. 6. Maximum octahedral shear stress for the plate across the thickness for $\mu_2/\mu_1 = 2.0$, $\nu_1 = \nu_2 = 0.33$ and different values of a/h.

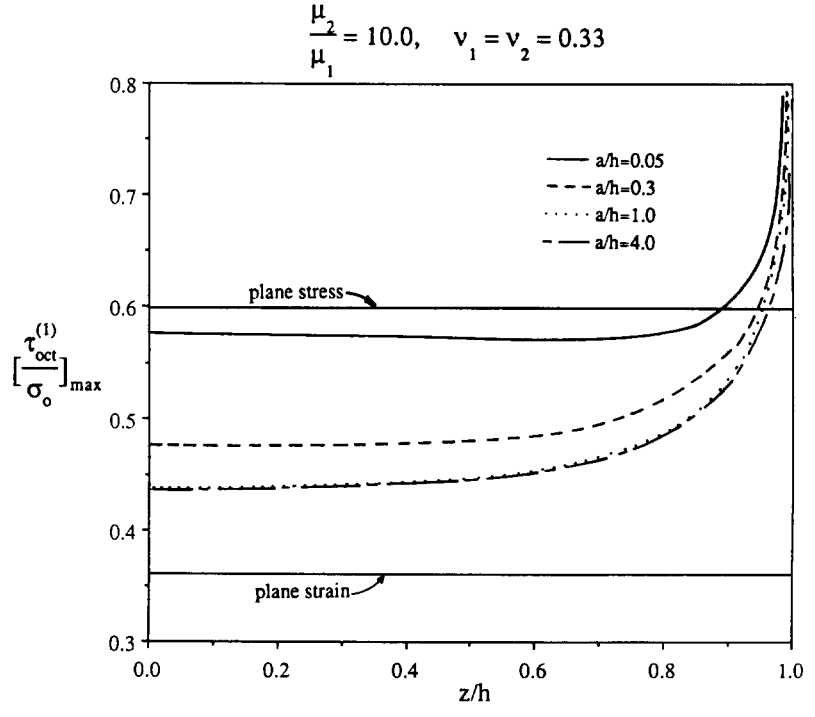

Fig. 7. Maximum octahedral shear stress for the plate across the thickness for $\mu_2/\mu_1 = 10.0$, $\nu_1 = \nu_2 = 0.33$ and different values of a/h.

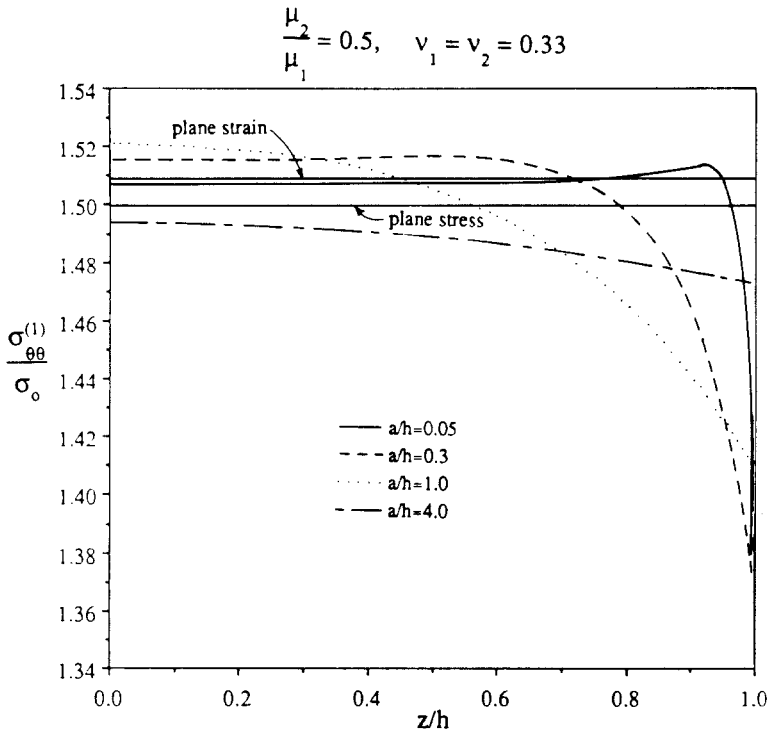

Fig. 8. Stress $\sigma_{\theta\theta}$ for the plate across the thickness at $r = a, \theta = \pi/2$ for $\mu_2/\mu_1 = 0.5$, $\nu_1 = \nu_2$ 0.33 and different values of a/h.

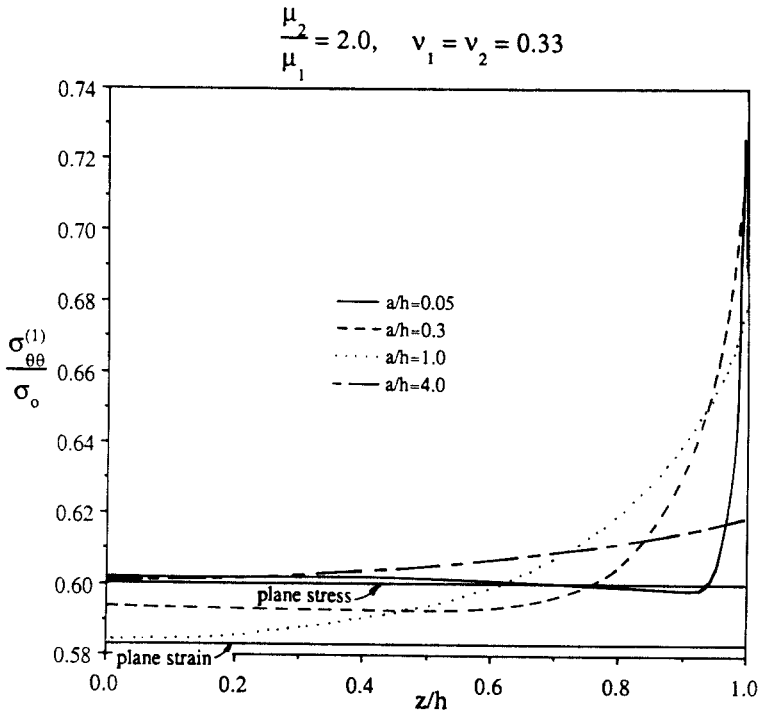

Fig. 9. Stress $\sigma_{\theta\theta}$ for the plate across the thickness at $r = a, \theta = \pi/2$ for $\mu_2/\mu_1 = 2.0$, $\nu_1 = \nu_2 = 0.33$ and different values of a/h.

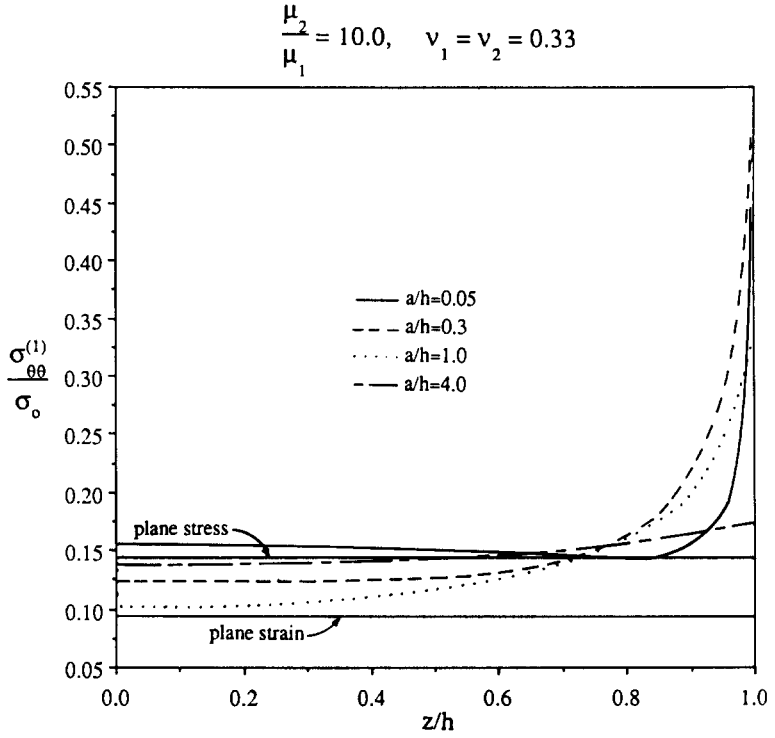

Fig. 10. Stress $\sigma_{\theta\theta}$ for the plate across the thickness at $r = a$, $\theta = \pi/2$ for $\mu_2/\mu_1 = 10.0$, $\nu_1 = \nu_2 = 0.33$ and different values of a/h.

if the inclusion is of a softer material, or at $\theta = \pi/2$ if the inclusion is of a stiffer material. Three important observations can be made from these figures. First, for thick plates ($a/h = 0.05$) the plane strain solution always gives nonconservative approximations to the three-dimensional solution in the interior of the plate. Second, in the neighborhood of $z/h = 1.0$ and for $\mu_2/\mu_1 = 2.0, 10.0$, the stresses become high, which is compatible with the stress singularities predicted in [10] for $\mu_2/\mu_1 > 1.0$. It should be noted that the plane strain solution fails to predict these singularities for it neglects the three-dimensional effects. Third, as a/h becomes large (thin plates) the three-dimensional solution tends to the plane stress solution.

Figures 8–13 show the stresses σ_{00} and σ_{zz} for the plate at $r = a$, $\theta = \pi/2$ as a function of z/h and illustrate how individual stresses vary across the plate thickness. Finally, Figs. 14 and 15 show the displacement u_{zz} at the surface of the plate ($z = h$) along the radial line $\theta = \pi/2$.

5. Conclusions

In view of the foregoing results, the following conclusions may be drawn.

(1) Thickness as well as the material properties play a fundamental role on the failure mechanism of a plate with a cylindrical inclusion. The thickness parameter, a/h, and the shear moduli ratio, μ_2/μ_1, control not only the maximum load that can be applied to the plate, but also the location where failure initiation may occur.

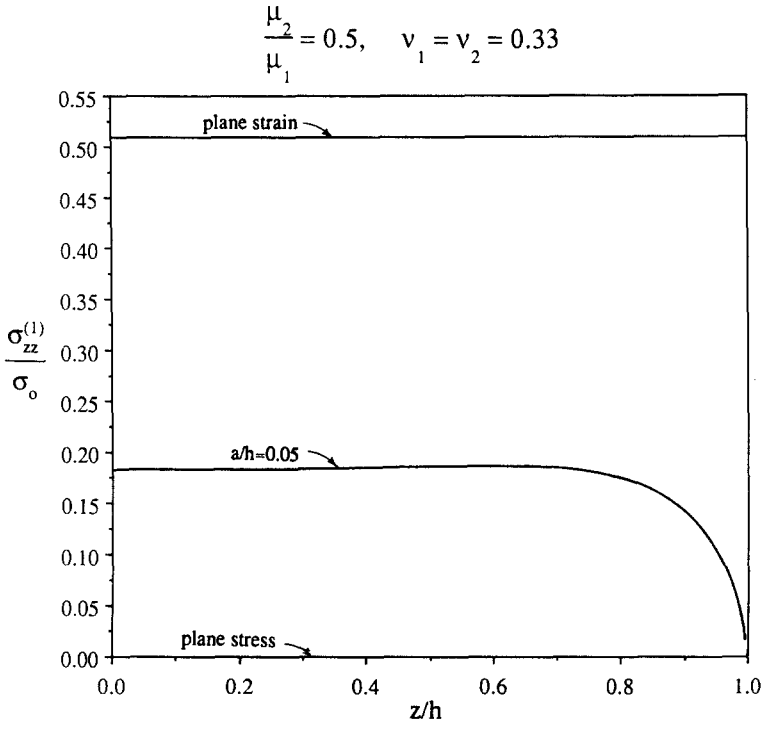

Fig. 11. Stress σ_{zz} for the plate across the thickness at $r = a$, $\theta = \pi/2$ for $\mu_2/\mu_1 = 0.5$, $\nu_1 = \nu_2 = 0.33$ and $a/h = 0.05$.

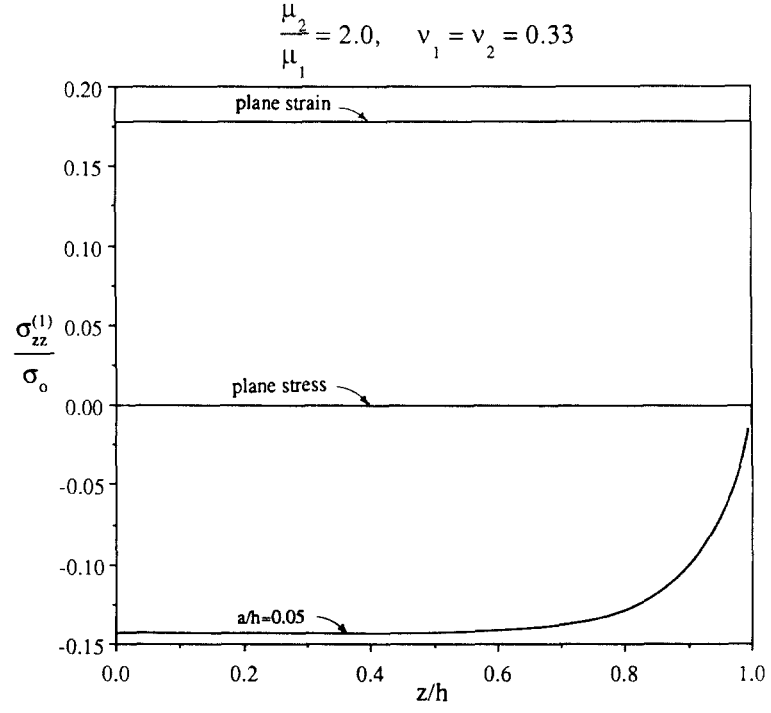

Fig. 12. Stress σ_{zz} for the plate across the thickness at $r = a$, $\theta = \pi/2$ for $\mu_2/\mu_1 = 2.0$, $\nu_1 = \nu_2 = 0.33$ and $a/h = 0.05$.

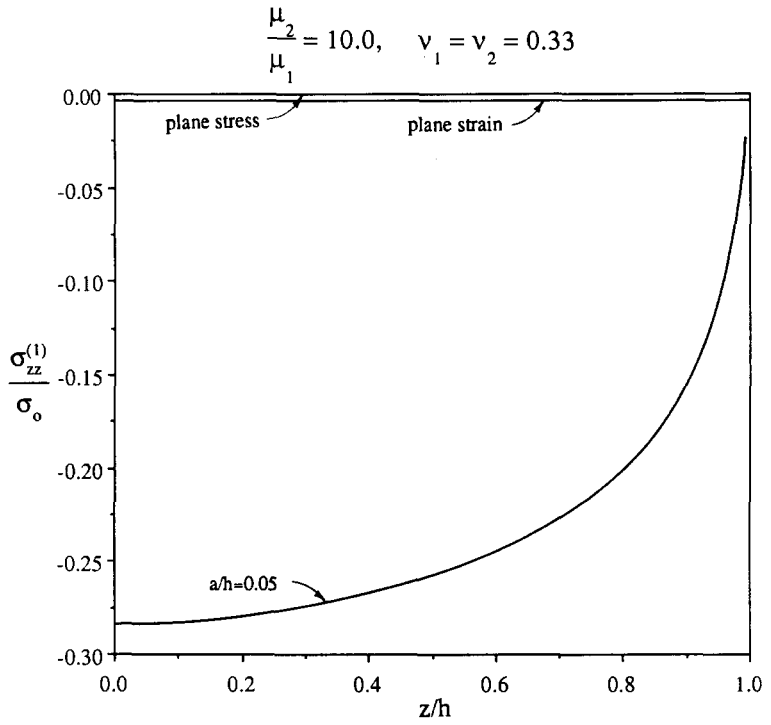

Fig. 13. Stress σ_{zz} for the plate across the thickness at $r = a, \theta = \pi/2$ for $\mu_2/\mu_1 = 10.0, \nu_1 = \nu_2 = 0.33$ and $a/h = 0.05$.

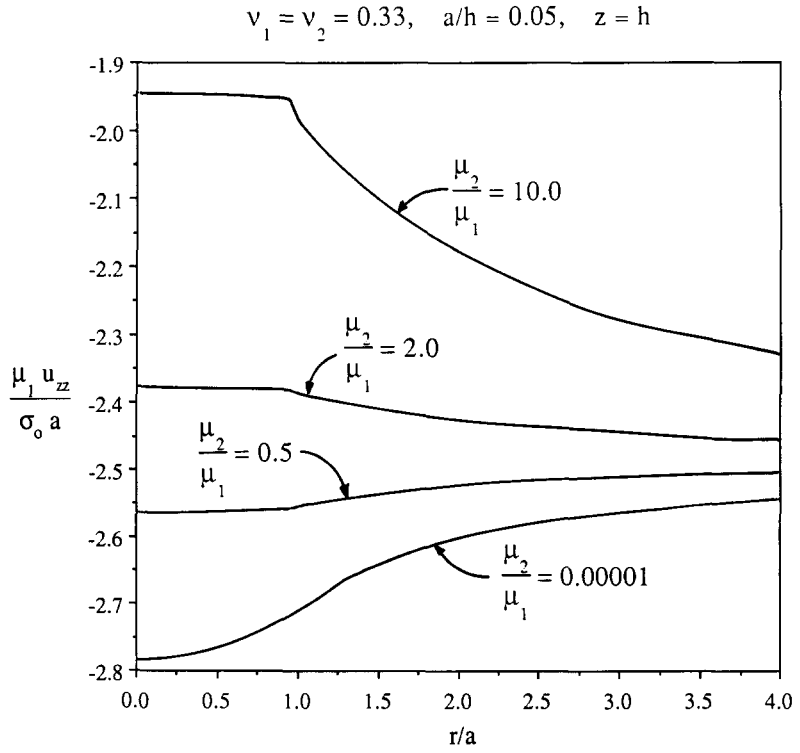

Fig. 14. Displacement u_{zz} as a function of r at $z = h, \theta = \pi/2$ for $a/h = 0.05, \nu_1 = \nu_2 = 0.33$ and different values of μ_2/μ_1.

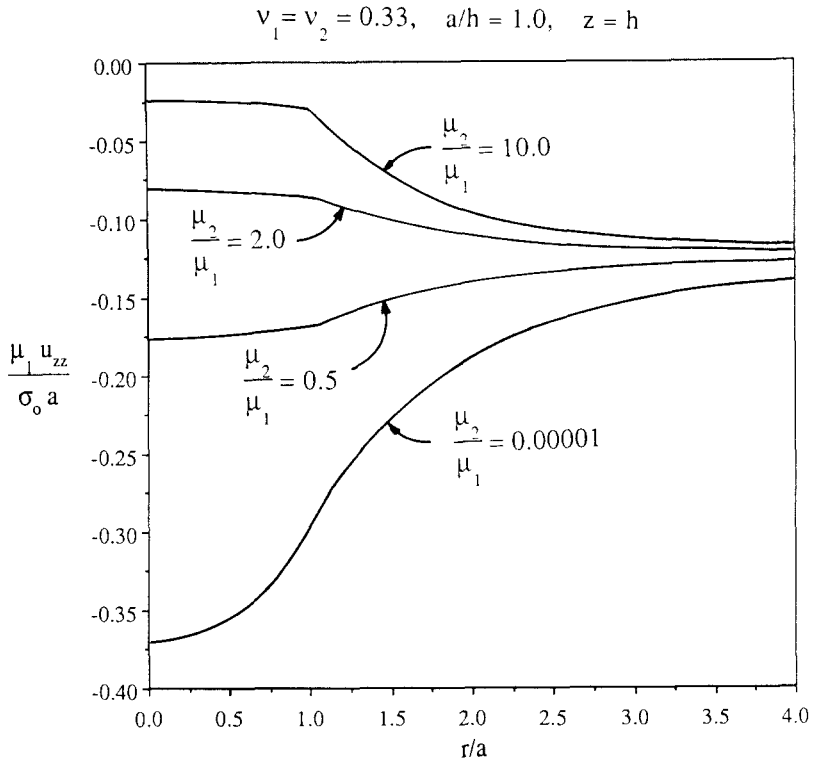

Fig. 15. Displacement u_{zz} as a function of r at $z = h, \theta = \pi/2$ for $a/h = 1.0$, $\nu_1 = \nu_2 = 0.33$ and different values of μ_2/μ_1.

(2) It is observed that for relatively thick plates and shear moduli ratios of $\mu_2/\mu_1 > 1$ the stresses are singular at the intersection of the cylindrical inclusion and the free surface of the plate. The strength of these singularities, however, is best if it is extracted by analytical means (see [10]).

(3) For relatively thick plates, the maximum octahedral shear stress predicted by the plane strain solution is always lower than the corresponding three-dimensional solution.

(4) As $h \to 0$, the plane stress solution is recovered.

(5) Finally, the plane stress solution is a good approximation for plates with ratios of $(a/h) \geqslant 4$.

Acknowledgments

This work was supported in part by the Air Force Office of Scientific Research Grant No. AFOSR-87-0204. The authors would like to thank Lt. Col. G. Haritos for this support. Also, the authors would like to acknowledge the time on the CRAY supercomputer at San Diego donated by the National Science Foundation.

References

1. R. Muki and E. Sternberg, *International Journal of Solids and Structures* 6 (1970) 69–90.
2. V.K. Luk and L.M. Keer, *International Journal of Solids and Structures* 15 (1979) 805–827.

3. J.N. Goodier, *Journal of Applied Mechanics, Transactions ASME* 55 (1933) 39–44.
4. I.W. Yu and G.P. Sendeckyj, *Journal of Applied Mechanics* 41 (1974) 215–221.
5. K. Suyehiro, "The distribution of stress in a tension strap having a circular hole filled with a plug," *The Society of Mechanical Engineers*, Japan (1914).
6. E.G. Coker and L.N.G. Filon, in *A Treatise on Photoelasticity*, Cambridge (1931) 497–500.
7. L.M. Keer, J. Dundurs and K. Kiattikomol, *International Journal of Engineering Science* 11 (1973) 1221–1233.
8. D.B. Bogy, *Journal of Applied Mechanics Transactions* ASME 35 (1968) 460–466.
9. V.L. Hein and F. Erdogan, *International Journal of Fracture Mechanics* (1971) 317–330.
10. E.S. Folias, *International Journal of Fracture* 39 (1989).
11. E.S. Folias, *Journal of Applied Mechanics* 42 (1975) 663–674.
12. E.S. Folias and J.J. Wang, "On the Three-dimensional Stress Field Around a Circular Hole in a Plate of Arbitrary Thickness", *Proceedings of the 19th, Midwestern Mechanics Conference*, Columbus, Ohio, September 1985. Also *University of Utah Technical Report*, May 1986.
13. L.V. Kantorovich and V.I. Krylov, *Approximate Methods of Higher Analysis*, Noordhoff, Holland (1964).
14. F.E. Penado, and E.S. Folias, "The Three-Dimensional Stress Field Around a Cylindrical Inclusion in a Plate of an Arbitrary Thickness," Interim Report, College of Engineering, University of Utah, September 1987.

Résumé. On résoud par voie analytique les équations de Navier à trois dimensions relatives au cas d'une inclusion cylindrique de rayon "a" noyée dans une tôle d'épaisseur arbitraire $2h$. On suppose que les matériaux constituant l'inclusion et la tôle sont homogènes et isotropes, et qu'ils ont des propriétés mécaniques différentes. Une liaison parfaite de leur interface est également supposée. La mise en charge est réalisée par une tension uniforme appliquée dans le plan de la tôle, en des point suffisamment distants de l'inclusion.

L'analyse montre que toutes les contraintes comprises dans l'octoèdre des tensions de cisaillement sont influencées par le rapport a/h et par les propriétés des matériaux. A la limite, lorsque le rapport des modules de cisaillement de l'inclusion et de la tôle tend vers zéro, ou vers un, on retrouve respectivement les résultats relatifs à un trou circulaire et à une plaque continue. De même, on retrouve la solution d'état plan de contrainte lorsque $a/h \to \infty$, ce qui serait le cas d'une tôle très mince. En outre, lorsque le rapport des modules est supérieure à un, les résultats numériques confirment la présence d'une singularité de contrainte près du point d'intersection de l'inclusion et de la surface libre de la tôle.